



ZnO-based varistors prepared by spark plasma sintering

Y. Beynet^a, A. Izoulet^{a,c}, S. Guillemet-Fritsch^a, G. Chevallier^a, V. Bley^b, T. Pérel^b, F. Malpiece^c, J. Morel^c, C. Estournès^{a,*}

^a CIRIMAT UMR CNRS 5085, Université Paul Sabatier, 118 route de Narbonne, 31062 Toulouse Cedex 9, France

^b LAPLACE, Université Paul Sabatier, 118 route de Narbonne, 31062 Toulouse Cedex 9, France

^c TRIDELTA Parafoudres S.A., Boulevard de l'Adour, 65202 Bagnères de Bigorre Cedex, France

Received 30 May 2014; received in revised form 7 October 2014; accepted 9 October 2014

Abstract

Varistor ceramics were prepared by spark plasma sintering (SPS) using two doped zinc oxide based powders. Optimized sintering cycle for the commercial powder (mixture of oxides) yielded dense parts (>99%) containing mainly ZnO grains (1 μm) and additional Bi₂O₃ and Zn₇Sb₂O₁₂ oxides. Sintering at the low oxygen partial pressure inherent to SPS leads to the reduction of Bi₂O₃ into metallic Bi. To reduce the grain size, improve the distribution of dopants and the grain size distribution, we used co-precipitation to synthesize a powder with the same formulation as the commercial powder. Due to the high reactivity of this powder, fully dense parts were obtained at temperature as low as 400 °C under air atmosphere using carbide tools. Such conditions led to limited ZnO grain growth and bismuth reduction during the thermal cycle. The fine microstructure obtained led to varistances with high electrical properties (threshold field higher than 2300 V/mm).

© 2014 Elsevier Ltd. All rights reserved.

Keywords: Varistor; Spark plasma sintering (SPS); Doped ZnO; Electrical properties

1. Introduction

In order to make the new generation of aircraft more economical and thus more competitive and for the protection of the environment, manufacturers have sought to reduce aircraft weight by introducing a large proportion of composites. With the use of these new types of materials, the flow of charges during lightning strike will be much less effective than with the use of traditional conductive materials. It is therefore necessary to provide better protection for the electronic devices on board. As a result, more compact and efficient varistors must be developed. A varistor is an electronic component with highly nonlinear current–voltage characteristics. In 1979, Mahan et al.¹ explained this highly nonlinear behaviour by electron tunnelling triggered by hole creation in the doped ZnO. In 1987, Dorlanne et al. brought a different approach to explain the phenomenon of conduction by the action of holes without considering a tunnelling effect.²

Moreover, Emtage³ has shown that the mean breakdown voltage per grain in the ceramic is less than that of an isolated grain boundary.

It was therefore necessary to prepare ceramics with a thinner microstructure than those already available on the market.^{4–6} Indeed, such a microstructure yields a larger number of grain boundaries per unit volume and hence allows the production of components with identical performances to those currently on the market, but with a lower weight and volume.

To achieve this target, spark plasma sintering (SPS), known to increase the kinetics of material densification, to reduce the sintering temperature and as a consequence to control the grain growth, has been considered.^{7–10} Kougo et al. studied the spark plasma sintering of non-doped zinc oxide.¹¹ They showed that the grain size of the ceramics obtained increases (1 to 100 μm) with sintering temperature (450 to 1200 °C) and consequently their electrical resistivity decreases. Misawa et al. studied the influence of current flow through ZnO samples during SPS.¹² The internal temperature of the sample and its electrical resistance were monitored during the sintering cycle. It was shown that a temperature difference of 200 K occurs between the

* Corresponding author. Tel.: +33 561556109; fax: +33 561556163.
E-mail address: estournes@chimie.ups-tlse.fr (C. Estournès).

specimen (T_s) and the sintering die (T_d) during the time of maximum temperature ($T_s > T_d$). Ning et al. used an extrusion tool with SPS to obtain ZnO films, with a c-axis preferred orientation, in order to improve the component's performances.¹³ Using this technique, they managed to reach a large number of grain boundaries per unit length suggesting future implementation of ceramics of lower thickness but with identical electrical properties.

Using SPS, some authors have already densified pure ZnO and Bi₂O₃ doped ZnO nanopowders.¹⁴ They observed a Bi₂O₃ reduction phenomena when the sintering temperature reached 600 °C, resulting in the appearance of Bi metal mainly at grain boundaries. The authors found out that this reduction is perfectly reversible by post-annealing the ceramics in air at 650 °C for 10 h. The coefficient of nonlinearity of these samples was low (between 3.6 and 5.8) as a consequence of the simple binary composition.

To induce the “varistor” behaviour in ZnO-based ceramics a heavy element with a large ionic radius has to be introduced.¹⁵ This heavy element is able to segregate at the grain boundary and to form an electronic conduction barrier between n-type semiconductive ZnO grains. Bismuth, a dopant present in most commercial varistors, acts at the grain boundary,¹⁶ due to the emergence of a liquid phase of Bi₂O₃ at approximately 820 °C that promotes grain growth during sintering. Particular attention has to be paid with bismuth because of its high volatility during the sintering process. Antimony, meanwhile, is a dopant that inhibits grain growth through the formation of spinel Zn₇Sb₂O₁₂ usually located at grain boundaries.¹⁷ Both nickel and antimony improve the stability of the varistor. Cobalt and manganese oxides cause an increase in the barrier height and the resistivity of the material.^{18,19}

In the present study, a ZnO powder doped with Sb₂O₃, Bi₂O₃, Co₃O₄, NiO and Mn₂O₃ as in the preparation of commercial varistors by Tridelta Parafoudres Co. Ltd. was densified by SPS. A second powder, of the same composition, but synthesized by coprecipitation, was studied. The aim of this work was to obtain a doped powder with a smaller ZnO grain size and distribution and better dopant homogeneity. Both powders were sintered by SPS and the structure and microstructure of the two sets of ceramics was determined and correlated to their electrical properties.

2. Experimental procedures

First, ZnO powder doped with Bi, Sb, Co, Mn and Ni was prepared by co-precipitation of an oxalate precursor. A schematic representation of the synthesis is shown in Fig. 1. The starting materials for the synthesis of doped Zn oxalate precursor were zinc nitrate (Zn (NO₃)₂·6H₂O, 98%, Alfa Aesar), bismuth nitrate (Bi (NO₃)₂·5H₂O, 98%, Alfa Aesar), cobalt nitrate Co(NO₃)₂·6H₂O, 98%, Alfa Aesar), manganese nitrate (Mn(NO₃)₂·6H₂O, 98%, Alfa Aesar), nickel nitrate (Ni(NO₃)₂·6H₂O, 98%, Fluka) and antimony trichloride (SbCl₃, 99% Merck). Solution 1 was prepared by dissolving Zn, Bi, Co, Mn and Ni salts in deionized water. Bismuth nitrate was dissolved in 1 M HNO₃ before adding it to solution 1. The acidic pH avoided precipitation of basic bismuth nitrate. The

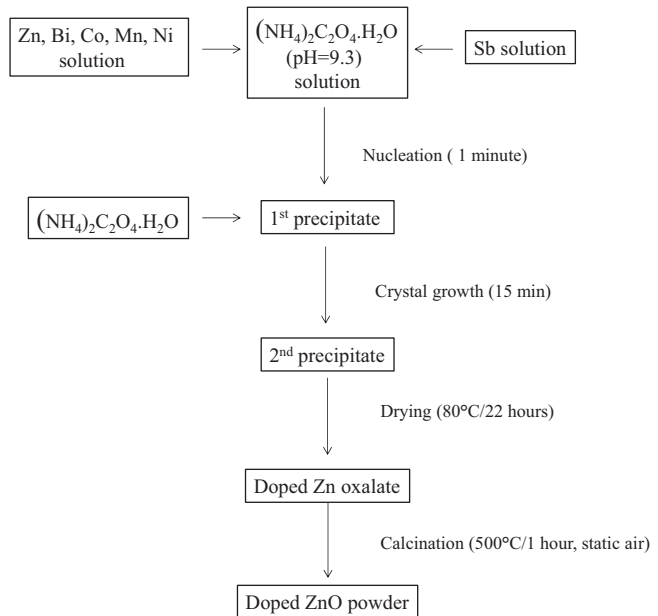


Fig. 1. Schematic representation of the synthesis.

metal concentration was fixed at 4 M. Solution 2 was prepared by dissolving antimony chloride in 4 M hydrochloric acid. Two solutions of 0.2 M ammonium oxalate ((NH₄)₂C₂O₄·H₂O) were used as precipitants. The pH of one of them was adjusted to 9.3 by adding NaOH. This gave a pH of around 7 at the end of the precipitation reaction which promotes the smallest and most homogeneous ZnO grain size.²⁰ Solutions 1 and 2 were introduced simultaneously into this ammonium oxalate solution to initiate nucleation. After stirring for 1 min, the second solution of ammonium oxalate was added. This second precipitation promoted crystal growth. After stirring for 15 min, the precipitates were washed with deionized water and dried at 80 °C for 22 h. IPC analyses confirm that the powder synthesized had the same composition as the commercial powder. The precursors were calcinated in ambient atmosphere at 500 °C for 1 h in static air. The calcinated powder was ground and sieved.

The samples were sintered using a Dr Sinter 2080 spark plasma sintering apparatus (Sumitomo Coal Mining Co. Ltd., Japan) available at the “Plateforme Nationale CNRS de Frittage Flash” (PNF2-CNRS) located at Toulouse (France). The powder was introduced in an 8 or 20 mm inner diameter graphite or tungsten carbide die lined with 0.2 mm thick graphite foil (Papyex-Mersen) then pre-compacted and placed in the SPS chamber. A pulse sequence of 12:2 was applied to heat the sample. The temperature was monitored using a thermocouple in a hole 1.8 mm in diameter and 3 mm deep located at the external surface of the die. Uniaxial pressure was applied at room temperature or at the dwell temperature.

The structure and the nature of the phases present in the powder and the ceramics were determined by X-ray diffraction (XRD) using a Bruker D4 Endeavor X-ray diffractometer. The powder and the ceramics were observed by scanning electron microscopy (SEM). The grain size, the morphology of the powder as well as the phase distribution and the microstructure of the ceramics were determined using a Jeol 6510LV microscope.

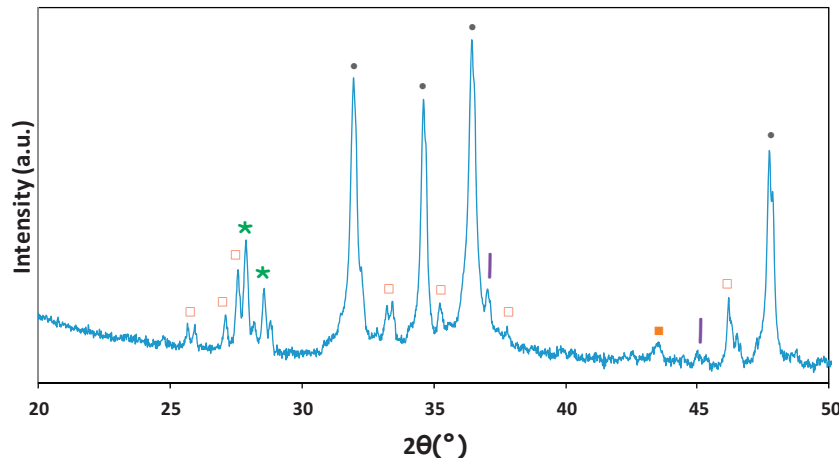


Fig. 2. X-Ray diffractogram of the commercial powder (●ZnO, □ Bi_2O_3 , ★ Sb_2O_3 , | Co_3O_4 , ■ NiO). (For interpretation of the references to colour in this figure legend, the reader is referred to the web version of this article.)

The rate of densification of the ceramics after sintering was evaluated by using a hydrostatic balance (Kern ARJ 220-4M) and by geometric measurements (when the sample had a densification lower than 92%).

Prior to electrical measurements, the pellet was slightly polished, and then gold electrodes (30 nm thick) were deposited by sputtering on each side of the pellet. The electrical characteristics of the varistors were studied using a source measure unit (SMU) Keithley 2410 or a high voltage generator FUG HCN 6.5 kV for voltages higher than 1100 V available at the LAPLACE laboratory. The threshold voltage V_S was measured for a current of 1 mA. The coefficient of nonlinearity α is defined by the following equation:

$$\alpha = \frac{\log(I_2/I_1)}{\log(V_2/V_1)} \quad (1)$$

where V_1 and V_2 are the electric fields corresponding to $I_1 = 1 \text{ mA}$ and $I_2 = 10 \text{ mA}$. The leakage current I_f was measured for a voltage equal to $V_S/2$.

3. Results

3.1. Commercial powder

The commercial oxide powder was produced by Tridelta Parafoudres S.A. The dopants present in the ZnO phase were Sb_2O_3 , Bi_2O_3 , Co_3O_4 , NiO and Mn_2O_3 . For confidential reasons, the actual percentage of the dopants cannot be given.

The X-ray diffraction pattern of the initial powder (Fig. 2) shows the strong diffraction lines of the major ZnO phase and the weak lines of the four additional oxides: Sb_2O_3 , $\alpha\text{-Bi}_2\text{O}_3$, NiO and Co_3O_4 . Mn_2O_3 was present at levels below the limit of detection of the device.

SEM-FEG observations (Fig. 3) show a heterogeneous morphology and an obvious wide grain size distribution, with grain sizes ranging from 0.3 to 1 micron.

In order to obtain dense ceramics at low temperatures, the sintering was carried out by spark plasma sintering (SPS). Several parameters of the sintering procedure were optimized,

i.e. the dwell temperature ($700 < T < 1100^\circ\text{C}$), the dwell time ($0 < t < 15 \text{ min}$), the compacting pressure ($50 < P < 130 \text{ MPa}$) applied at room temperature or at the dwell temperature, the sintering atmosphere (vacuum or argon), the heating rate (100 or $200^\circ\text{C}/\text{min}$).

Fig. 4 shows how the relative density of the ceramics varied as a function of the sintering temperature. An optimum relative density between 99 and 100% was obtained for a sintering temperature of 870°C .

For each temperature, the other parameters were varied, and the structure and the microstructure of the ceramics checked. The heating rate, the applied pressure, and the sintering atmosphere (vacuum or argon) had a relatively low influence on the composition and the microstructure of the ceramics. The ceramics were characterized by X-ray diffraction analyses. Three phases can be identified: ZnO, $\text{Zn}_7\text{Sb}_2\text{O}_{12}$ and metallic Bi (Fig. 5). Metallic Bi results from the reduction of Bi_2O_3 . Indeed, the use of a graphite die implies working at low oxygen partial pressure (under vacuum or inert gas) to prevent its degradation. At high temperature this then leads to the reduction of part of the Bi_2O_3 into metallic bismuth.¹⁴ The presence of metallic Bi is of

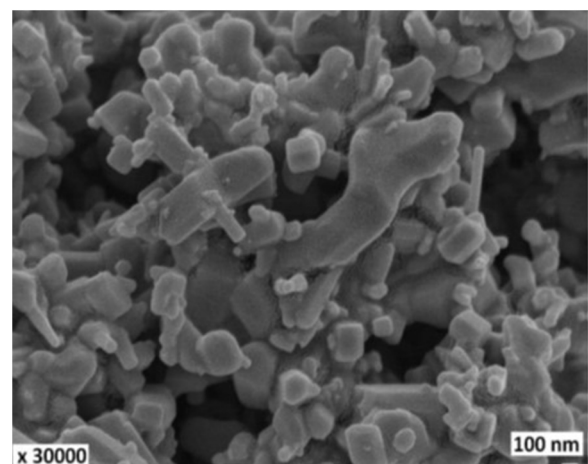


Fig. 3. SEM micrographs of the commercial powder.

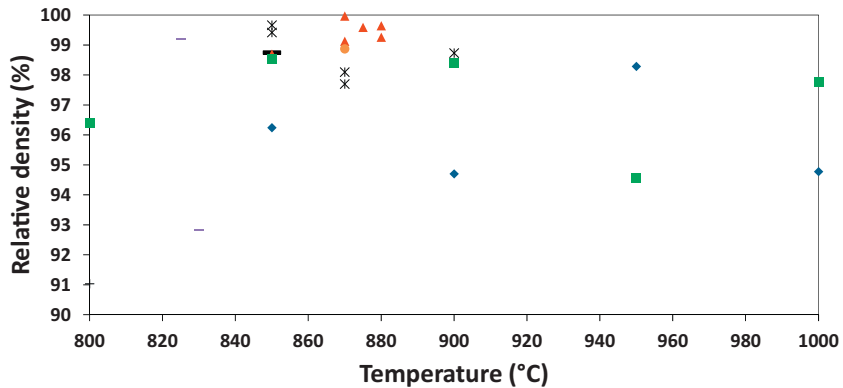


Fig. 4. Variation of the relative density of the ceramics obtained versus the sintering temperature, for various conditions (◆: 100 MPa under vacuum 5 min 100 °C/min Load applied at room temperature, ■: 100 MPa under vacuum 0 min 100 °C/min Load applied at dwell temperature, ▲: 100 MPa under vacuum 0 min 100 °C/min Load applied at room temperature, *: 100 MPa under vacuum 1 min 100 °C/min Load applied at room temperature, +: 100 MPa under vacuum 15 min 100 °C/min Load applied at room temperature, -: 50 MPa under vacuum 5 min 100 °C/min Load applied at room temperature, —: 100 MPa under vacuum 0 min 200 °C/min Load applied at room temperature, ○: 100 MPa Ar 0 min 100 °C/min Load applied at room temperature, ■: 100 MPa Ar 5 min 100 °C/min Load applied at room temperature). (For interpretation of the references to colour in this figure legend, the reader is referred to the web version of this article.)

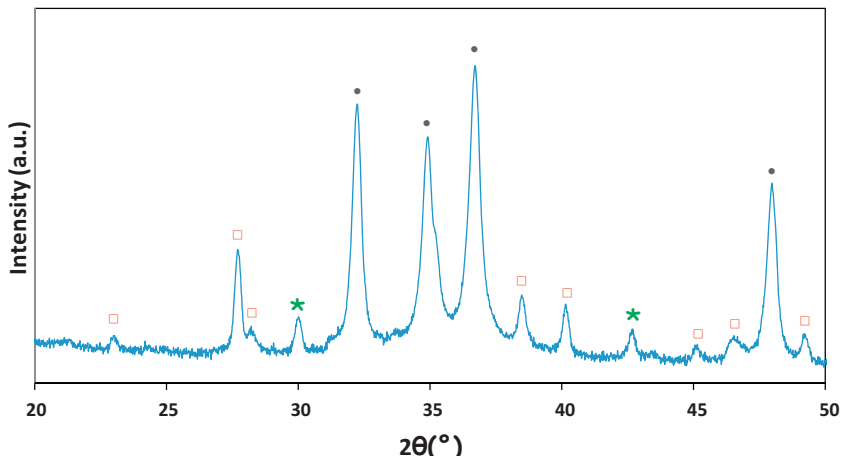


Fig. 5. XRD diffractogram of ceramics sintered SPS at 870 °C (●ZnO, □Bi, ★Zn₇Sb₂O₁₂). (For interpretation of the references to colour in this figure legend, the reader is referred to the web version of this article.)

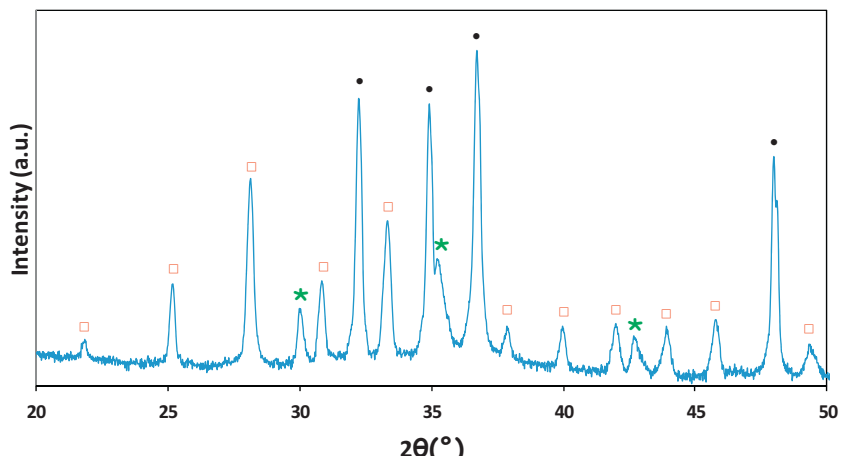


Fig. 6. XRD diffractogram of ceramics sintered by SPS at 870 °C and annealed at 750 °C (●ZnO, □Bi₂O₃, ★Zn₇Sb₂O₁₂). (For interpretation of the references to colour in this figure legend, the reader is referred to the web version of this article.)

course not desired in the formulation because it is a conductor. In order to reoxidize metallic Bi into Bi_2O_3 , the ceramics are then annealed in air. Previous work showed that metallic Bi present in doped ZnO sintered by SPS¹⁴ can be reoxidized into Bi_2O_3 after annealing in air at 750 °C for 10 h at a heating rate of 1 °C/min. In fact, three phases are observed: ZnO , Bi_2O_3 and $\text{Zn}_7\text{Sb}_2\text{O}_{12}$ after annealing the samples under the same conditions (Fig. 6).

SEM observations of the pellets sintered at 870 °C under vacuum, with dwell times of 0, 1 and 15 min, a heating rate of 100 °C/min and cold compaction at 100 MPa are shown on Fig. 7. The zinc oxide phase exhibits grain sizes of about 1 μm, 4 μm and 8 μm, respectively, for dwell times of 0, 1 and 15 min. Moreover, small grains, about a few tens of nanometres, were observed and identified by EDS analyses as the $\text{Zn}_7\text{Sb}_2\text{O}_{12}$ phase. BS-SEM observation on polished sample sintered at 870 °C under vacuum, without dwell time, a heating rate of 100 °C/min and cold compaction at 100 MPa (Fig. 8) shows the three phases characteristics of a varistor: the ZnO grain appear in dark gray, spinel phase in light gray and the bright elements are Bi_2O_3 . Unfortunately the microstructure (grain size and phase distribution) is less visible than on the fractured samples presented on Fig. 7 of the article. We have attempted several conditions for both chemical and thermal etching on the dense samples to reveal the grain boundaries without any success due to the high volatility of the Bi_2O_3 species.

3.2. Co-precipitated powder

In order to reduce the grain size and the grain size distribution and to improve the distribution of dopants, an oxide powder of the same composition as the commercial powder, was obtained by co-precipitation followed by calcination. Fig. 9 shows the microstructure of the calcinated powder. The grains have a regular, more or less cubic shape. The average grain size is approximately 700 nm. At high magnification, crystallites of about 20 nm are visible in the grains.

X-Ray diffraction (XRD) of the co-precipitated powder (Fig. 10) shows the zinc oxide phase and two antimony oxide phases (Sb_2O_3 and Sb_2O_4). The two antimony oxide forms were explained by Peiteado et al., as they have shown that at 500 °C Sb_2O_3 is oxidized into Sb_2O_4 ($\text{Sb}_2\text{O}_3 + 1/2\text{O}_2 \rightarrow \text{Sb}_2\text{O}_4$).²¹ In our case, Sb_2O_3 was not completely oxidized. The other dopants i.e. Bi_2O_3 , Co_3O_4 , NiO and Mn_2O_3 were not detected by X-Ray diffraction analyses. The larger width of the peaks of the synthesized powder, compared with the commercial powder, indicates smaller crystallite size.

At first, the powder obtained by the chemical route was sintered by SPS using the same conditions as those established for commercial powder (870 °C, no dwell, applied pressure of 100 MPa, vacuum). During the sintering, thermal shrinkage was monitored by a dilatometer. Fig. 11 shows the sintering profiles of both powders. The densification of the commercial powder starts at 700 °C, while the shrinkage of the synthesized powder starts at temperatures as low as 200 °C. The lower temperature of

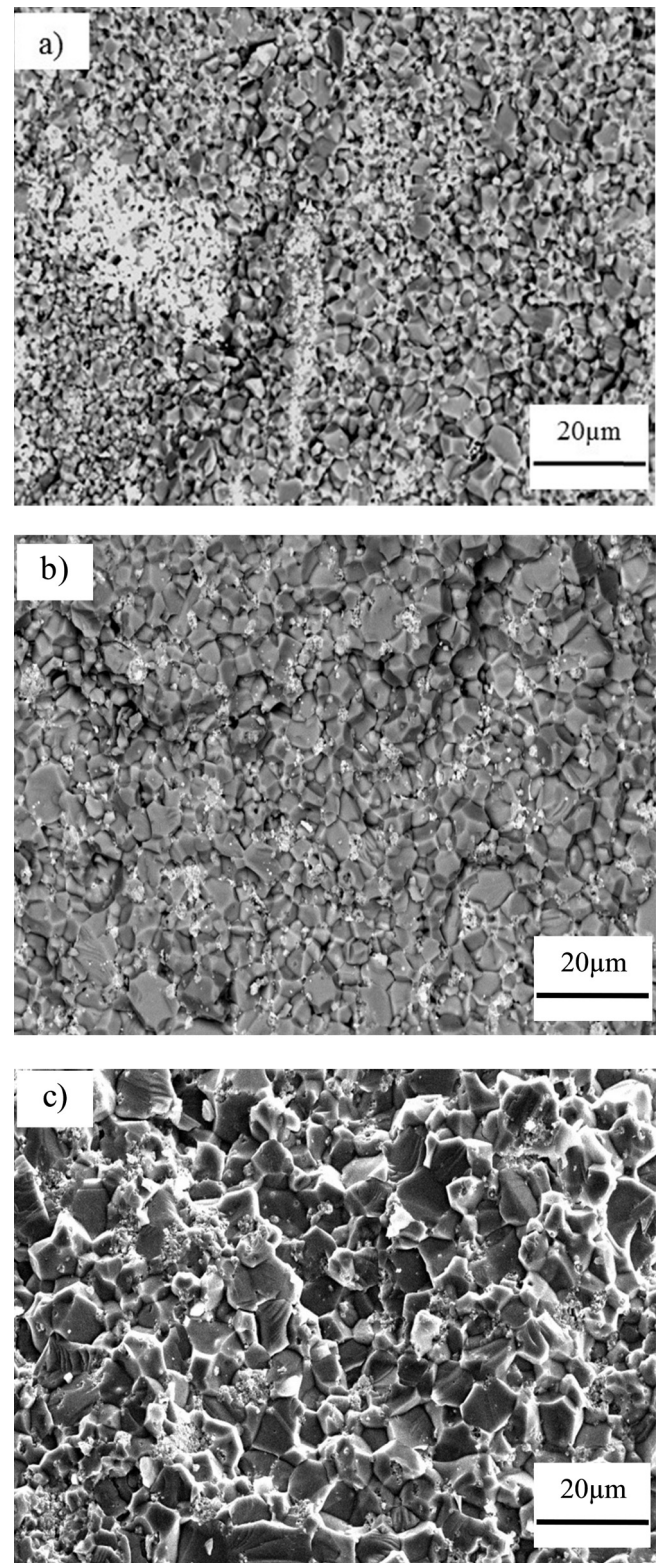


Fig. 7. SEM micrographs fracture of pellets sintered at 870 °C with a dwell time of (a) 0 min (b) 1 min(c) 15 min.

the onset of densification start was explained by the smaller grain size of the synthesized powder, involving higher densification.

The thermal shrinkage curves showed that it was possible to sinter the synthesized powder at very low temperatures. In

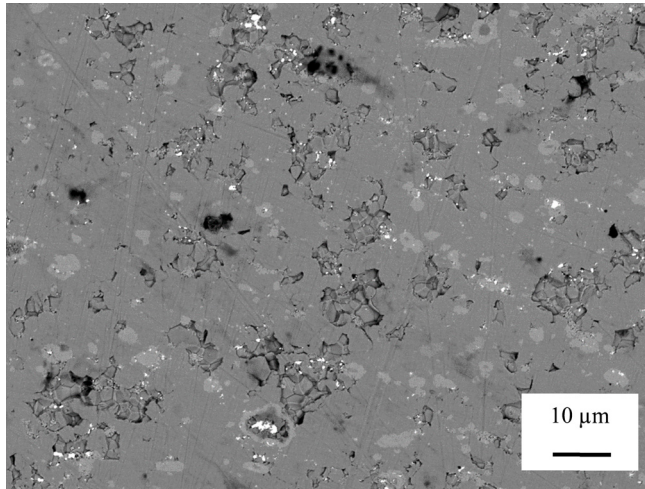


Fig. 8. BS SEM polished micrograph of pellet made from commercial powder sintered at 870 °C, 100 MPa and 0 min under vacuum atmosphere.

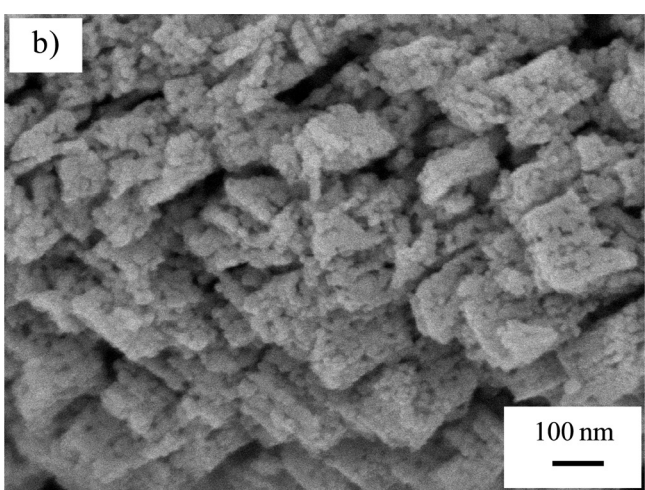
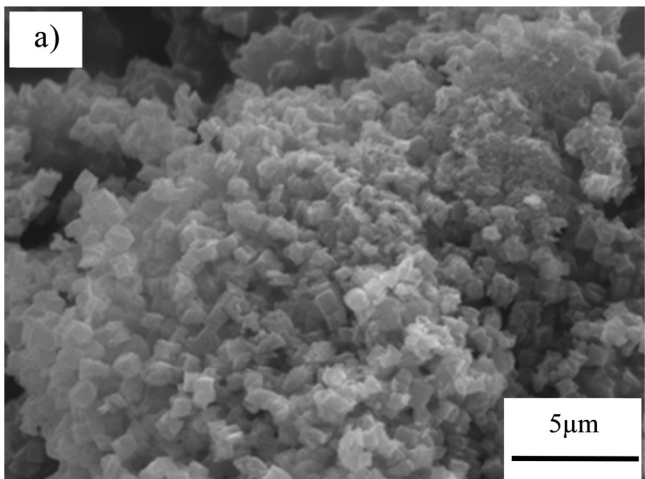


Fig. 9. SEM (a) and FEG-SEM (b) micrographs of the doped ZnO co-precipitated powder.

Table 1

Densification of the synthesized powder sintered under air atmosphere.

Sintering temperature (°C)	Dwell time (min)	Pressure (MPa)	Density (g/cm ³)	Densification (%)
400	3	500	5.45	96.5
500	3	250	5.50	97.3
600	3	250	5.56	98.4

In this case, three sintering temperatures were chosen: 400 °C, 500 °C and 600 °C, with a dwell time of 3 min. Decreasing the sintering temperature involved increasing the compacting pressure (250 MPa and 500 MPa) to obtain dense samples. High compacting pressure implied the use of a tungsten carbide die, known to be pressure resistant. Then, sintering could be performed under air atmosphere, and the reduction of bismuth oxide into metallic bismuth should be avoided. However the X-Ray diffraction analyses carried out on the pellets still showed the peak of metallic Bi (Fig. 12), but smaller. It was therefore still necessary to anneal the pellet after sintering to reoxidize the metallic Bi. Moreover, the X-Ray diffraction analyses indicated the ZnO phase and the spinel phase Zn₇Sb₂O₁₂ (Fig. 12). It can be noted that a temperature of 400 °C is not enough to allow complete reaction between Sb₂O₄ and ZnO to form the spinel phase.

The densifications of the pellets are high, between 96 and 98%, whatever the sintering conditions (Table 1). SEM observations (Fig. 13) were performed on the pellet sintered at 600 °C. The ceramic grain size ranged from 0.3 to 0.6 μm, which was lower than that of pellets prepared from the commercial powder (1 μm). This ceramic with such small grain size is obtained due to the moderate growth of the crystallites occurring at so low sintering temperature. Fig. 14 BS-SEM observation on polished pellet sintered at 600 °C. This image shows the ZnO grains in gray and the Bi-rich phases in white.

4. Electrical characterization

4.1. Influence of the dwell time during sintering of the commercial powder

The electrical characteristic curve log J (current density) vs log E (electrical field) obtained at room temperature for the pellet sintered by SPS at 870 °C, with a dwell time ranging from 0 to 15 min, with a pressure of 100 MPa and subsequently annealed in air at 750 °C for 10 h is reported in Fig. 15. A varistor effect is clear. Indeed, a strong nonlinear behaviour is seen in a wide range of voltages with a significant change in slope. The main electrical characteristics are reported in Table 2.

The electrical field decreases as the grain size increases. Indeed, if grains are smaller, there are more ZnO grains per unit volume and so, more potential barriers per unit volume. This characteristic is particularly interesting because it shows that the threshold field can be optimized by controlling the dwell time.

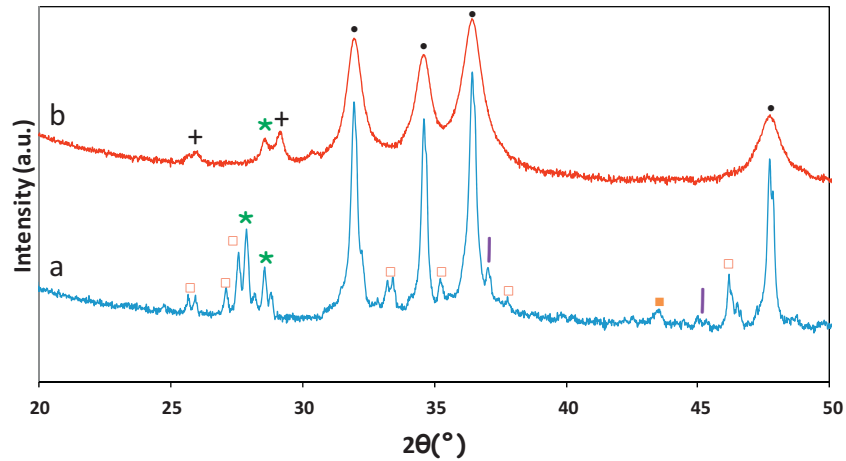


Fig. 10. X-Ray diffractograms of (a) commercial powder (●ZnO, □Bi₂O₃, ★Sb₂O₃, |Co₃O₄, ■NiO) and (b) synthesized powder (●ZnO, ★Sb₂O₃, +Sb₂O₄). (For interpretation of the references to colour in this figure legend, the reader is referred to the web version of this article.)

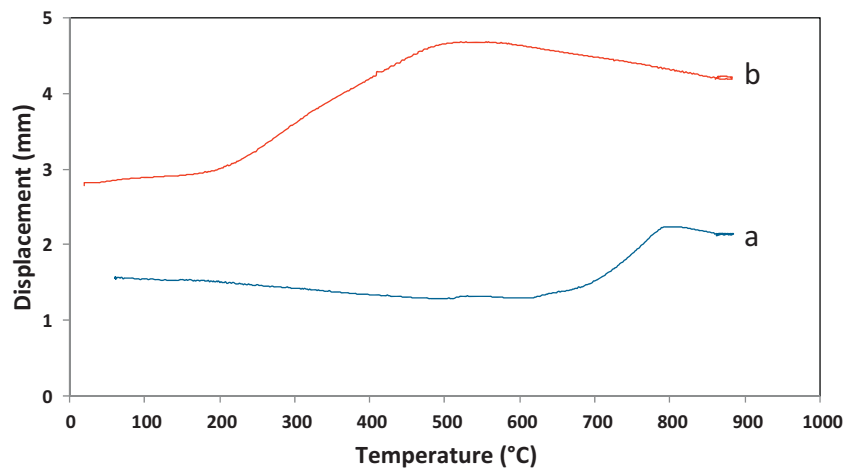


Fig. 11. Sintering profiles of (a) commercial powder (b) synthesized powder.

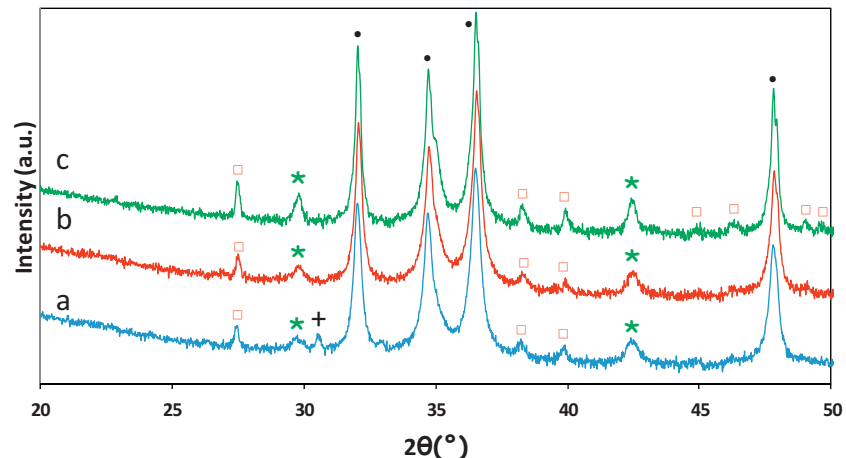


Fig. 12. XRD diffractograms of pellets made from synthesis powder sintered by SPS at (a) 400 °C 500 MPa, (b) 500 °C 250 MPa (c) 600 °C 250 MPa (●ZnO, □Bi, ★Zn₇Sb₂O₁₂, +Sb₂O₄). (For interpretation of the references to colour in this figure legend, the reader is referred to the web version of this article.)

Table 2

Electrical characteristics of the commercial powder sintered with different dwell times.

Sintering temperature (°C)	Dwell time (min)	Pressure (MPa)	Grain size (μm)	E^* (V/cm)	α	I_f (nA)
870	0	100	1	880	27	1900
870	1	100	4	500	50	1430
870	15	100	8	260	37	1070

* E : breakdown field.

Table 3

Electrical characteristics of the commercial and the synthesized powder sintered in different conditions.

Powder	Sintering T (°C) Dwell time (min) Pressure (MPa)	Annealed T (°C)/t(h)	Grain size (μm)	E^* (V/cm)	α	I_f (nA)
Commercial	870/1/100	750/10	1–2	880	27	1900
Synthesized	870/1/100	750/10	2–3	1182	28	2440
Synthesized	600/3/250	580/10	0.3–0.6	>2300		

* E : breakdown field.

4.2. Influence of the powder and the SPS parameters

In order to improve the characteristics of the varistor, a ZnO based powder was synthesized and sintered by SPS at low temperature (600 °C) under air atmosphere. Varistors with very small grains were prepared. The electrical characteristics curve of these varistors is reported in Table 3 and Fig. 16. This figure also reports the characteristics of the commercial and the synthesized powder sintered at higher temperatures (870 °C).

The varistors prepared from the synthesized powders and sintered at low temperature presented an electrical field that was significantly higher than that of ceramics prepared from commercial powders. A value of more than 2300 V/cm (this value was limited by the equipment used) was noted in the varistor sintered at 600 °C. In the case of varistors sintered at 870 °C, those obtained from the synthesized powder showed a

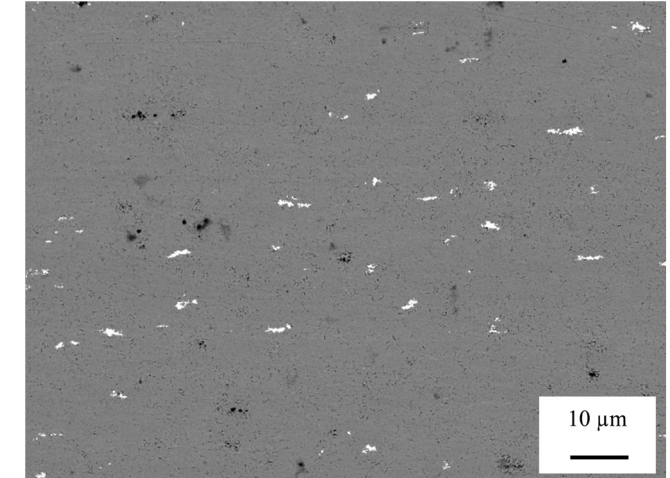
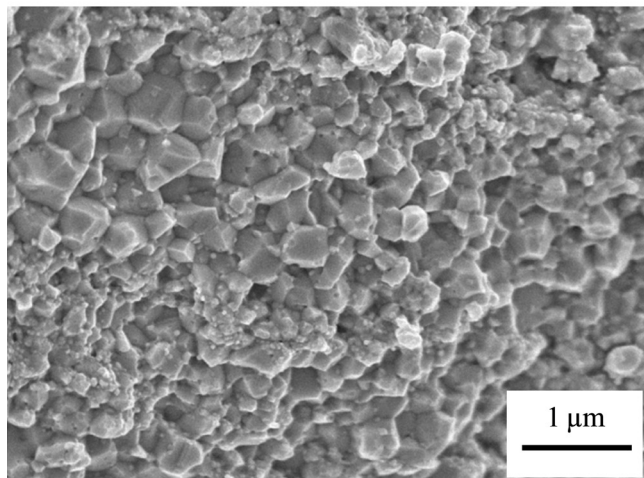
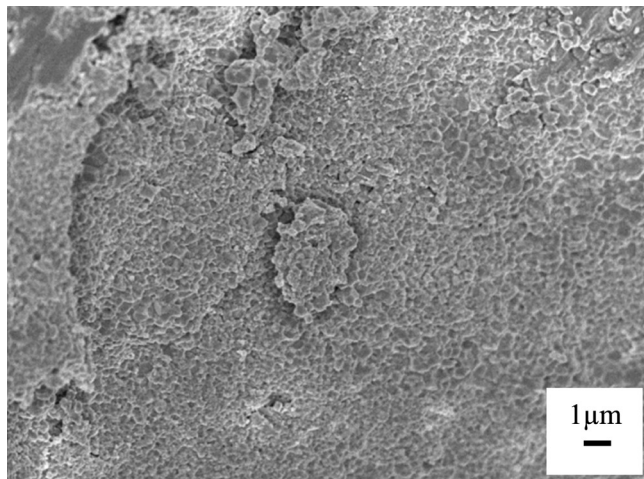


Fig. 13. SEM fracture micrographs of pellets made from synthesized powder sintered at 600 °C and 250 MPa.

Fig. 14. BS SEM polished micrograph of pellet made from synthesized powder sintered at 600 °C, 250 MPa and 3 min under air atmosphere.

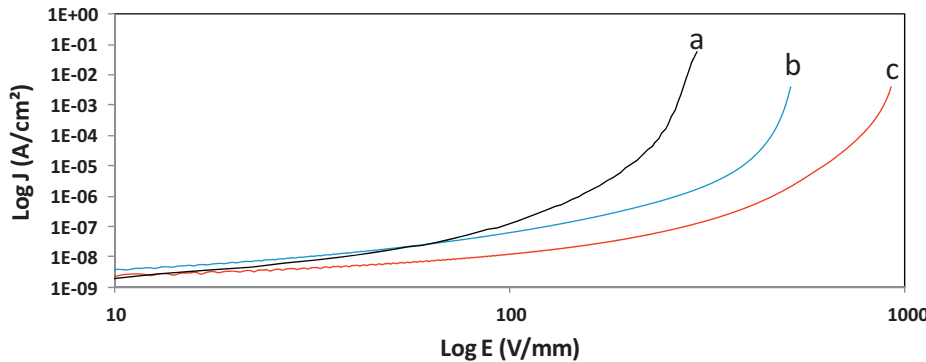


Fig. 15. E - J characteristics of pellets sintered at 870 °C with a dwell time of: (a) 15 min, (b) 1 min and (c) 0 min.

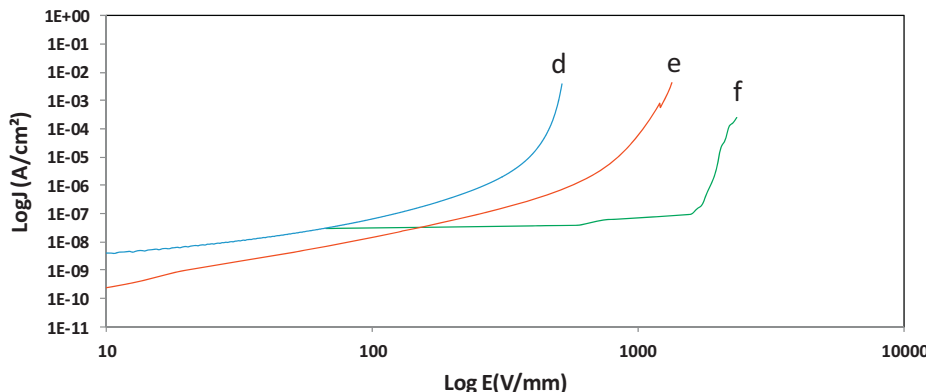


Fig. 16. E - J characteristics of pellets sintered by SPS: (d) commercial powder SPS sintered (870 °C, 100 MPa, 1 min) under vacuum, (e) synthesized powder SPS sintered (870 °C, 100 MPa, 1 min) under vacuum, and (f) synthesized powder SPS sintered (600 °C, 250 MPa, 3 min) under air atmosphere.

higher breakdown voltage than those prepared from the commercial powder, although its grain size was higher. The more homogeneous dopant distribution in the ceramic probably explains this result.

5. Conclusion

Nano-sized ZnO-doped powder was synthesized by coprecipitation. It was sintered by SPS at low temperature, i.e. 600 °C, with high compaction pressure (250 MPa) and under an air atmosphere. Sintering of small grains at low temperature yielded varistors with very low grain size: 300–600 nm. In this case, the threshold field was increased from 880 V/mm to more than 2300 V/mm. Controlling the grain size allowed the threshold field to be optimized.

Acknowledgements

These research works were made within the framework of the project PREFACE (Project of Study Lightning on more Electric Composite Plane). The authors would like to thank the projects leaders ASTECH: Hispano-Suiza, AESE: Safran Engineering Service, PEGASE: Eurocopter, and the DGE and Region Midi-Pyrénées for their financial support under Grants No. 08-2-93-0744. The support of the Plateforme nationale CNRS de frittage flash was gratefully appreciated.

References

- Mahan GD, Levinson LM, Philipp HR. Theory of conduction in ZnO varistors. *J Appl Phys* 1979;50:2799–812.
- Dorlanne O, Tao T. The grain junction in zinc oxide varistors. *High Technol Ceramics* 1987;38:1809–17.
- Emtage PR. Statistics and grain size in zinc oxide varistors. *J Appl Phys* 1979;50:6833–7.
- Gupta TK. Application of zinc oxide varistors. *J Am Ceram Soc* 1990;73:1817–40.
- Bartkowiak M, Mahan GD, Modine FA, Alim MA, Lauf R, McMillan A. Voronoi network model of ZnO varistors with different types of grain boundaries. *J Appl Phys* 1996;80:6516–22.
- Özgür Ü, Alivov YI, Liu C, Teke A, Reshchikov MA, Doğan S, et al. A comprehensive review of ZnO materials and devices. *J Appl Phys* 2005;98:41301.
- Chaim R, Levin M, Shlauer A, Estournès C. Sintering and densification of nanocrystalline ceramic oxide powders. A review. *Adv Appl Ceram* 2008;27:159–69.
- Estournès C, Oquab D, Selezneff S, Boidot M, Monceau D, Grossin D, et al. Shaping of nanostructured materials or coatings through spark plasma sintering. *Mater Sci Forum* 2012;70:6–709 (24–30).
- Chaim R, Marder R, Estournès C, Shen Z. Densification and preservation of the ceramic nanocrystalline character by spark plasma sintering. *Adv Appl Ceram* 2012;111(5&6):280–5.
- Orru R, Licheria R, Mario Locci AM, Cincotti A, Cao G. Consolidation/synthesis of materials by electric current activated/assisted sintering. *Mater Sci Eng Res* 2009;63:127–287.
- Kougo T, Yoshikawa A. Fabrication and characterization of polycrystalline bulk ZnO with large grain size of similar to 100 μm by the spark plasma sintering. *Phys Status Solidi C* 2006;3:785–8.

12. Misawa T, Shikatani N, Kawakami Y, Enjoji T, Ohtsu Y, Fujita H. Observation of internal pulsed current flow through the ZnO specimen in the spark plasma sintering method. *J Mater Sci* 2009;**44**:1641–51.
13. Ning JL, Jiang DM, Kim KH, Shim KB. Influence of texture on electrical properties of ZnO ceramics prepared by extrusion and spark plasma sintering. *Ceram Int* 2007;**33**:107–14.
14. Saint Macary L, Kahn ML, Estournès C, Fau P, Trémouilles D, Bafleur M, et al. Size effect on properties of varistors made from zinc oxide nanoparticles through low temperature spark plasma sintering. *Adv Funct Mater* 2009;**19**:1775–83.
15. Tsai JK, Wu TB. Nonohmic characteristics of ZnO–V₂O₅ ceramics. *J Appl Phys* 1994;**76**:4817–22.
16. Greuter F, Blatter G. Electrical properties of grain boundaries in polycrystalline compound semiconductors. *Semicond Sci Technol* 1990;**5**:111–37.
17. Peiteado M, Fernandez JF, Caballero AC. Processing strategies to control grain growth in ZnO based varistors. *J Eur Ceram Soc* 2005;**25**:2999–3003.
18. Onreabroy W, Sirikulrat N. Effects of cobalt doping on nonlinearity of zinc oxide. *Mater Sci Eng B—Adv* 2006;**130**:108–30.
19. Hong YW, Kim JH. The electrical properties of Mn₂O₃ doped ZnO. *Ceram Int* 2004;**30**:1301–6.
20. Mory JE, Guy I, Schneider D, Rousset A, Legros R, Peigney A. Doped zinc oxide powder, preparation thereo and ceramic produced there from. Patent WO1994022765 A1. 1994.
21. Peiteado M, De la Rubia MA, Fernandez JF, Caballero AC. Thermal evolution of ZnO–Bi₂O₃–Sb₂O₃ system in the region of interest varistors. *J Mater Sci* 2006;**41**:2319–25.